Nonlinear evolution of Alfvén waves and particle acceleration in space

R. P. Sharma, H. D. Singh and M. Malik

Centre for Energy Studies, Indian Institute of Technology Delhi, New-Delhi-110016, India

Abstract. We present a numerical simulation leading to the formation of intense magnetic filaments of kinetic Alfvén waves (KAWs) in steady state when the nonlinearity arises due to ponderomotive effects and Joule heating. When the plain KAW is perturbed by a transverse perturbation and the magnitude of the pump KAW changes, chaotic filamentary structures of magnetic field have been observed. At higher KAW pump wave amplitude, the spectra approaches near the Kolmogorov $k^{-5/3}$ scaling at small spatial scales which steepens to a $\sim k^{-2}$ form towards larger spatial scales. The motion is found to be quasiperiodic and chaotic for different parametric regimes. Relevance of these studies in magnetosphere and solar wind for particle acceleration has also been pointed out.

Index Terms. Alfvén waves, chaos, magnetic filaments, magnetosphere, solar wind.

_____

1. Introduction

In space physics the nonlinear properties of finite amplitude Alfvén waves are of great interest, largely due to the fact that there have been a great many observations of these waves in the solar wind, and in the Earth's magnetosphere and ionosphere. Many have studied the Earth's space environment including formation of discrete auroral arcs (Atkinson, 1970; Miura and Sato, 1980), and generation of MHD waves and field line resonance (Laysak, 1991). At the equatorial magnetosphere, where the magnetospheric plasma is hot and the electron thermal speed exceeds the Alfvén speed ($v_{te} = \sqrt{T_e/m_e} > v_A$), the kinetic Alfvén wave (KAW) is the appropriate limit. The KAW appears in an intermediate beta plasma with $m_e/m_i < \beta \left(= 8\pi n_0 T / B_0^2\right) < 1$.

Cluster spacecraft observations (Sundkvist et al., 2005) in the high altitude cusp found KAWs with frequencies less than the ion gyrofrequency and non-potential ion-cyclotron waves (electromagnetic ion-Bernstein waves) above the ion gyrofrequency. Existence of small-scale, large amplitude KAWs/spikes at the plasma sheet boundary layer at auroral regions of altitudes of 4-6 R_E were presented from Polar spacecraft observations (Wagant, 2000).

Some observations (Stasiewicz, 1997; Louran, 1994) by the Freja and Fast Auroral SnapshoT (FAST) spacecrafts showed that the physical nature of strong electric spikes in the auroral ionosphere and magnetosphere, which are characterized by perturbed electric and magnetic fields can be explained in terms of KAW.

The small-scale KAWs are generated from the large scale Alfvén waves through one or more of varieties of mechanisms which have been proposed to result in the filamentation of large amplitude Alfvén waves. Filamentation of Alfvén waves could become relevant in the observations of Cluster spacecraft in magnetosheath regions close to the bow shock (Alexandrova *et al.*, 2004). The present paper focuses on the filamentation process arising on account of the coupling between the main KAW and the perturbation that leads to wave energy concentration in magnetic filaments. Effect of these coherent structures on particle acceleration has also been pointed out.

To develop a fully numerical solution of KAW filamentation in steady state when the nonlinearity arises due to ponderomotive effects and Joule heating, the envelope nonlinear dynamical equation satisfies the modified nonlinear Schrödinger (MNLS) equation. It turns out that by changing the parameter governing the pump wave amplitude, this MNLS equation numerically brings the chaotic structures in the filamentation process.

In particular, the question of how nonlinear Alfvén waves evolve into Alfvén turbulence has been achieved by studying the Alfvénic chaos. For nondissipative (Hamiltonian) Alfvén systems, Hada and Kennel (1990) showed that the system dynamics near the phase-space (soliton) separatrix becomes chaotic as the driver amplitude increases. W. Horoton (1997) studied solar wind driven dynamics of the magnetosphere and found a highly complex and chaotic orbits in the ion motion in the high pressure-to-magnetic pressure reversed field current. The nonlinear dynamics of KAW turbulence

caused by the three-wave interaction among KAWs and its application to the Earth's magnetosphere were studied by Voitenko (1998).

2. Model equations

In an intermediate β ($m_e/m_i < \beta < 1$) plasma magnetized by a uniform ambient magnetic field B_0 along the z direction, the dynamical equation governing the propagation (in the x-z plane) of low frequency, long wavelength, finite amplitude KAW, can be obtained by using the standard method (Shukla and Stenflo, 1999, 2000; Shukla and Sharma, 2002; Shukla and Sharma et al., 2004) and written as

$$i\frac{\partial B_y}{\partial z} + 2i\Gamma\frac{\partial B_y}{\partial x} + \frac{\partial^2 B_y}{\partial x^2} + \frac{1}{2g}\left(e^{2g|B_y|^2} - 1\right)B_y = 0 \tag{1}$$

where $\partial_z B_y << k_z B_y$. Γ is a parameter characterizing the normalized perpendicular wavenumber in terms of electron's collisionless skin depth, given by

$$\Gamma = \left(v_{te}/v_A\right)k_{0x}\lambda_e \tag{2}$$

g is the parameter governing the pump wave amplitude. The normalizing values are $z_n = 2/k_{0z}$, $x_n = v_{te}\lambda_e/v_A$, and $B_n = \left[\{1-\eta(1+\delta)\}v_A^2 k_{0z}^2/16\pi n_0 T_e\omega^2\right]^{-1/2}$ where k_{0x} (k_{0z}) is the component of the wave vector perpendicular (parallel) to $\hat{\mathbf{z}}B_0$, c_s ($=\sqrt{T_e/m_i}$) is the ion sound speed, ω_{ci} ($=cB_0/m_i c$) is the ion gyrofrequency, c is the speed of light, λ_e ($=\sqrt{c^2 m_e/4\pi n_0^2}$) is the collisionless electron skin depth, n_0 is the unperturbed plasma number density, T_e represents the plasma electron temperature, $\eta = \omega^2/\omega_{ci}^2$, $\delta = m_e k_{0x}^2/m_i k_{0z}^2$, and $\omega(<< \omega_c)$ is the KAW frequency.
When $g = 0$, equation (1) is reduced to modified NLS equation, which was studied numerically by the same authors (Singh and Sharma, 2006). As $g \neq 0$, however, the integrability of Eq. (1) is broken and the spatial chaos are expected.

When $\Gamma = 0$, Eq. (1) admits the uniform-wave-train solution

$$B_{ys}(z) = B_{y0}e^{-iz} \tag{3}$$

where B_{y0} are

$$B_{y0} = 0, \pm\left[\frac{1}{2g}\ln(1-2g)^{-1}\right]^{1/2} \tag{4}$$

We assume the initial state to be B_{y0}.

The complex nonlinear evolution of KAW having a fixed Γ at z = 0 and an initial amplitude as

$$B_y(x,0) = B_{y0}\left(1 + \varepsilon\cos(\alpha x)\right) \tag{5}$$

is studied by using Eq. (1) in a periodic box. Here B_{y0} is the amplitude of the homogenous pump KAW, ε and α are the parameters which remain constant in the simulation. Before proceeding further, one can analyze this evolution in the linear regime by doing stability analysis. Therefore, this analysis can be done by following the standard procedure (Cramer and Watson, 1984). One can treat this problem as if we have a uniform plane KAW and perturbation is superimposed on it. In linearized form, Eq. (1) leads to the following dispersion relation:

$$K^2 - 4\Gamma\alpha K + 4\Gamma^2\alpha^2 - \alpha^4 + 2\alpha^2|B_{y0}|^2 e^{2g|B_{y0}|^2} = 0 \tag{6}$$

where the spatial propagating dependence is proportional to $\exp(-iKz)$. The linear growth rate as a function of perturbation wave number α can be calculated from

$$\gamma(\alpha) = -2i\alpha\Gamma + \alpha\sqrt{2|B_{y0}|^2 e^{2g|B_{y0}|^2} - \alpha^2} \tag{7}$$

where $K = i\gamma$. It is obvious that the purely growing case is recovered when $\Gamma = 0$, provided that the perturbation wave number α lies in the range

$$0 < \alpha < \alpha_{cr} = |B_{y0}|\left\{\sqrt{2}\exp\left(g|B_{y0}|^2\right)\right\} \tag{8}$$

The unstable wave number corresponding to the maximum instability is

$$\alpha_{\max} = |B_{y0}|\exp\left(g|B_{y0}|^2\right) \tag{9}$$

3. Numerical simulation

We solve Eq. (1) satisfied by KAW numerically, in a periodic box for the initial conditions of simulation as specified by Eq. (5). The pseudo-spectral method of simulation has been employed for transverse (x-direction) space integration with periodic length $L_x = 2\pi/\alpha$, and the predictor-corrector method for propagation along z-direction where α is the wave number ($\alpha_{\max}$) corresponding to the maximum instability mode. The linear evolution is exactly integrated which forms an important feature of the code to accurately reproduce the instability and a fixed step size in z ($\Delta z = 5\times 10^{-4}$) was used in order to monitor the invariants of NLS equation to the desired accuracy. The accuracy was determined by the constancy of the number $N = \sum_k|B_k|^2$ when $\Gamma = 0$ and $g = 0$. During the computation the conserved quantity was preserved to the order of 10^{-5} accuracy. The diagnostics were carried out at every $\Delta z = 0.01$ using 128 grid points. After testing this algorithm, we modified it for $\Gamma \neq 0$ and $g \neq 0$ case of equation (1).

When $g \neq 0$, Eq. (1) becomes more general MNLS equation which shows nearly integrable dynamics and irregular solution that exhibits the chaotic motion. The results of filament formation of KAW by changing the parameter g and keeping Γ (= 0.01) fixed are presented below.

Investigations of nonlinear dynamical systems both theoretical and experimental have shown that both relatively simple low-dimensional systems and highly complex infinite dimensional systems may evolve from a steady state to a chaotic state as a control parameter is increased.
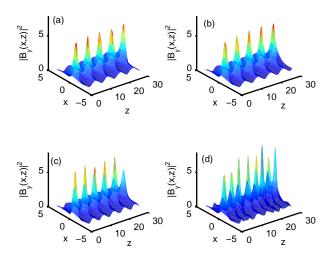

Fig. 1. The magnetic field intensity profile of KAW (a) g = 0.001, (b) g = 0.01, (c) g = 0.3, and (d) g = 0.05.

To have a detailed understanding we choose one typical case of MNLS equation when $\beta = 0.1$, at different g values. The magnetic-field intensity profiles of KAW with g = 0.001, 0.01, 0.03, and 0.05 are shown in Figs. 1(a)-1(d). It has been observed that magnetic filamentary structures are formed. Perturbation takes energy from the main KAW by nonlinear interaction, grows, and finally can form their own filaments. Therefore, the KAW breaks up into filamentary structures where the intensity is very high. When $g = 0.001$ the peaks of the filaments are of almost same intensity. As we increase the value of g, the peaks are of different intensity as seen from Fig. 1(d) when g = 0.05. The same authors have studied recently the filament formation when g = 0 (Singh and Sharma, 2006). They found that as the value of the normalized wave number increases from Γ = 0, the periodicity observed in filament formation was destroyed and the pattern was complex.

We construct the phase space diagrams $\left[\left| B_y (0,z) \right|, d \left| B_y (0,z) \right| / dz \right]$ and the results are presented in Figs.2(a)-2(d). As seen in phase space diagram, finite number of dots with irregular HMO crossings has been

observed. As the value of g increases, infinite number of dots filling up the substantial portions of phase space has been observed. The KAW field evolution from coherence to turbulence is spatially chaotic.

In order to study the effect of filament formation on the wave number spectrum, we have studied $\left| B_k \right|^2$ against k_z at a
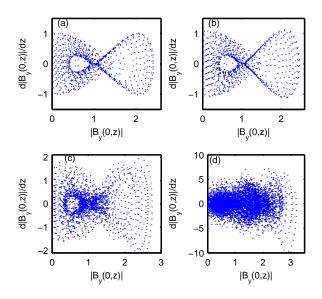

Fig. 2. Phase-space plots of KAW (a) g = 0.001, (b) g = 0.01, (c) g = 0.3, and (d) g = 0.05.

fixed x (= 0) value. Figs. 3(a)-3(d) present the power spectra $\left| B_k \right|^2$ against k_z. As the value of g increases, the negative exponent of k increases and the spectral intensity confined to lower wave number spreads to higher wave number. It appears that by further increasing the value of g = 0.05, the spectra approaches near the Kolmogorov $k^{-5/3}$ scaling at small spatial scales which steepens to a $\sim k^{-2}$ form towards larger spatial scales.

In addition, we also measure the largest Lyapunov exponent. It is seen from Fig. (4) that the largest Lyapunov exponent is positive for almost all the values of g used here; the system is defined to be chaotic. Thus KAW can exhibit chaotic dynamics giving rise to a turbulent component of the magnetic fluctuations. It shows that the degree of Alfvén chaos is a function of the parameter g.

We point out that our results can be quite useful to the understanding of nonlinear wave filamentation in the geosynchronous plasma environment (5-10 R_E), cusp region of magnetopause, as well as in the solar wind. First, we discuss the relevance of our work to the geostationary orbit, the orbital location where a body holds a fixed position relative to the rotating Earth, located at 6.6 R_E. The typical plasma parameters (Garrett and DeForest, 1979) in this

region are $B_0 \sim 200$ nT, $n_0 \sim 10$ cm^{-3}, T~1 Kev then $\beta \sim 0.1$, $v_A \sim 1.4 \times 10^8$ cm/s, $v_{te} = 1.3 \times 10^9$ cm/s, ω_{ci} =19.16 Hz, $\rho = 1.6 \times 10^6$ cm. The cusp is an important region in the Earth's magnetosphere where the solar wind can directly
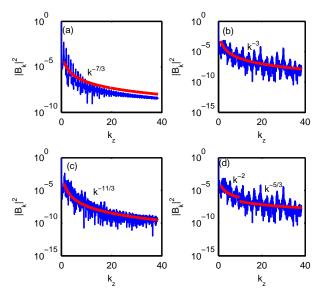
T=10ev; then $\beta \sim 0.335$, $v_A \sim 7.7 \times 10^6$ cm/s, $v_{te} = 1.3 \times 10^8$ cm/s, ω_{ci} =0.575 Hz, $\rho = 5.4 \times 10^6$ cm. The characteristic scale of the filament size for all the three cases is of the order of ρ in transverse direction and $10^3 \rho$ in propagation z-direction for lower value of g and as the value of g increases the filament size decreases nearly half.

Fig. 3. The power spectra of KAW (a) g = 0.001, (b) g = 0.01, (c) g = 0.3, and (d) g = 0.05. The thick line curve indicates the scaling.
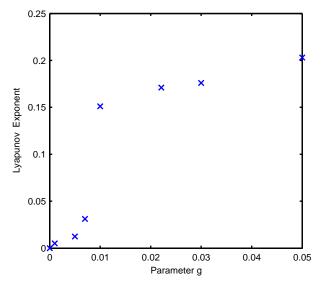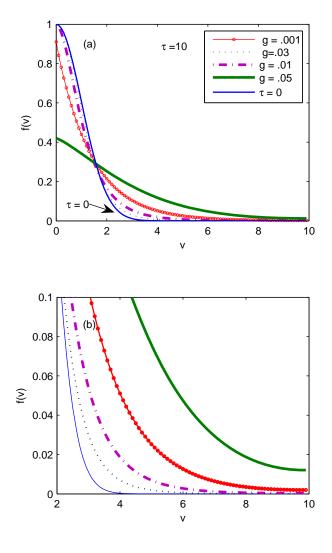

Fig. 4. Lyapunov exponent versus g.

Fig. 5. : Velocity distribution function: (a) at time τ=0 and τ= 10 for different values of g, (b) magnified view of the superthermal tail of (a).

access the ionosphere, and where large amounts of the plasma as well as kinetic and electromagnetic energies are transported. The typical plasma parameters (Sundkvist, 2005) in this region are $B_0 \sim 100$ nT, $n_0 \sim 5$ cm^{-3}, T=100 eV; then $\beta \sim 0.02$, $v_A \sim 9.9 \times 10^7$ cm/s, $v_{te} = 4.2 \times 10^8$, ω_{ci} = 9.58 Hz, $\rho = 10^6$ cm. Outside the Earth's magnetosphere, the typical values of several solar wind parameters (Cravens, 2004) as measured by Helios 2 at 1 AU are $B_0 \sim 6$ nT, $n_0 \sim 3$ cm^{-3},

Finally we have studied the evolution of the velocity distribution function due to localized field structures. The repeated interaction of the ions with the localized field can be described by the velocity space diffusion. The evolution of the velocity distribution function can be described by the Fokker- Plank equation given by

$$\frac{\partial f}{\partial t} = \frac{\partial}{\partial v}\left(D(v)\frac{\partial f}{\partial v} \right) \tag{10}$$

where $D(v)$ is the diffusion coefficient defined by

$$D(v) = \frac{1}{4}\left(\frac{e}{m_i}\right)^2 l_A \int dk \left|E_k\right|^2 \delta(\omega - kv)$$

$$= \frac{1}{4}\left(\frac{e}{m_i}\right)^2 l_A \left|E_k\right|^2_{k=\omega/v} \qquad (11)$$

The value of the $|E_k|$ for continuously changing k can be found from the overall shape of the Fourier spectrum. We use the approximate form $|E_k| = |E_{kmin}| |k_{min}/k|^{\eta/2}$ where η is the spectral index and l_A is the periodicity length.

Defining the scaled time $\tau = (v_{thi})^2/D_0$, and normalized the velocity by thermal velocity (v_{thi}) of ions , $D(v)$ by D_0 and $f(t,v)$ by $f(0,0)$, the normalized Fokker-Plank equation can be written as

$$\frac{\partial f}{\partial \tau} = \frac{\partial}{\partial u}\left(D(u)\frac{\partial f}{\partial u}\right) \qquad (12)$$

where D_0 is defined by

$$D_0 = \frac{1}{4}\left(\frac{e}{m_i}\right)^2 l_A \frac{\left|E_{k_{min}}\right|^2}{v_{k_{min}}} \qquad (13)$$

We proceed to solve the Eq. (12) numerically with the Maxwellian distribution as the initial condition. Fig. (5) displays the velocity distribution function at time $\tau = 0$ and for different values of g at $\tau = 10$. It is evident from the figure that the localized fields accelerate some ions and thus populating the super-thermal tail. Also the extent to which the superthermal tail will be populated is dependent on the g values.

4. Summary and discussion

We have investigated the filamentation instabilities of large-amplitude, KAWs propagating at an angle to the background magnetic field. The structures observed in the magnetosphere and solar wind can be generated by a nonlinear stage of kinetic Alfvén wave evolution which produces large scale structures and further collapses transversely to small scale structures which allows dissipation processes like ion-cyclotron resonance or Laundau damping to act, leading to the heating of the plasma. The localized fields accelerate some ions and thus populating the super-thermal tail.

References

G. Atkinson, "Auroral arcs: Result of the interaction of a dynamic magnetosphere with the ionosphere," *J. Geophys. Res.,* vol. 75, p. 4746, 1970.

O. Alexandrova, A. Mangeney, M. Maksimovic, *et al.,* "Cluster observations of finite amplitude Alfvén waves and small-scale magnetic filaments downstream of a quasi-perpendicular shock," *J. Geophys. Res.* vol. 109, A05207, 2004.

M. S. Cramer and L. T. Watson, "The evolution of long-wave solutions to the nonlinear Schrödinger equation," *Phys. Fluids,* vol. 27, pp. 821-826, 1984.

T. E. Cravens, *Physics of Solar System Plasmas*, Cambridge University Press, sec. ed. p. 3, 345, 2004.

H. B. Garrett and S. E. DeForest, "An analytical simulation of the geosynchronous plasma environment," *Planet. Space Sci.* vol. 27, pp. 1101-1109, 1979.

T. Hada, C. F. Kennel, B. Buti and E. Mjolhus, "Chaos in driven Alfvén systems," *Phys. Fluids B*, vol. 2, pp. 2581-2590, 1990.

W. Horton, "Chaos and structures in the magnetosphere," *Phys. Reports,* vol. 283, pp. 265-302, 1997.

P. Louarn, J. E. Wahlund, T. Chust, *et al.*, "Observation of kinetic Alfvén waves by FREJA spacecraft," *Geophys. Res. Lett.* vol. 21, pp. 1847-1850, 1994.

R. L. Lysak, "Feedback instability of the ionospheric resonant cavity," *J. Geophys. Res.,* vol. 96, pp. 1553-1568, 1991.

A. Miura and T. Sato, "Numerical simulation of global formation of auroral arcs," *J. Geophys. Res.*, vol. 85, pp. 73-91, 1980.

A. Shukla and R. P. Sharma, "Nonlinear kinetic Alfvén waves associated with saturating nonlinearity: application to solar wind and coronal heating," *J. Atm. Solar-Terresrial Phys.,* vol. 64, pp. 661-668, 2002.

A. Shukla, R. P. Sharma and Monika Malik, "Filamentation of Alfvén waves associated with transverse perturbation," *Phys. Plasmas,* vol. 11, pp. 2068-2074, 2004.

P. K. Shukla and L. Stenflo, "Plasma density cavitation due to inertial Alfvén wave heating," *Phys. Plasmas,* vol. 6, pp. 4120-4122, 1999.

P. K. Shukla and L. Stenflo, "Generation of localized density perturbation by shear Alfvén waves," *Phys. Plasmas,* vol. 7, pp. 2738-2739, 2000.

H. D. Singh and R. P. Sharma, "Numerical simulation of kinetic Alfvén waves to study filament formation and their nonlinear dynamics in solar wind and corona," *Phys. Plasmas,* vol. 13, 012902, 2006.

K. Stasiewicz, G. Gustafsson, G. Marklund, *et al..* "Cavity resonators and Alfvén resonance cones observed on Freja," *J. Geophys. Res.,* vol. 102, pp. 2565-2576, 1997.

D. A. Sundkvist, M. Vaivads, Andre, *et al.,* "Multi-spacecraft determination of wave characteristics near the proton gyrofrequency in high-altitude cusp," *Ann. Geophysicae.* vol. 23, pp. 983-995, 2005.

D. A. Sundkvist, Vladimir Krasnoselskikh, Padma. K. Shukla, et al., "*Insitu* multi-satellite detection of coherent vortices as a manifestation of Alfvénic turbulence," *Nature,* vol. 436, pp. 825-828, 2005.

Yu. M. Voitenko, "Three-wave coupling and weak turbulence of kinetic Alfvén waves," *J. Plasma Physics,* vol. 60, pp. 515-527, 1998.

J. R. Wygant, A. Keiling, C. A. Cattell, *et al.,* "Evidence for kinetic Alfvén waves and parallel electron energization at 4-6 RE altitudes in the plasma sheet boundary layer," *J. Geophys. Res.* vol. 107, p. 1201, doi: 10.1029/2001JA900113, 2002.